Les Cahiers du GERAD ISSN: 0711–2440

Nanoparticle optimization for enhanced targeted anti-cancer drug delivery

I. M. Chamseddine,
M. Kokkolaras

G–2017–57

July 2017

GERAD HEC Montréal
3000, chemin de la Côte-Sainte-Catherine
Montréal (Québec) Canada H3T 2A7

Tél. : 514 340-6053
Téléc. : 514 340-5665
info@gerad.ca
www.gerad.ca

Nanoparticle optimization for enhanced targeted anti-cancer drug delivery

Ibrahim M. Chamseddine [a]
Michael Kokkolaras [b]

[a] *Department of Mechanical Engineering, McGill University, Montréal (Québec), Canada, H3A 0C3*

[b] *GERAD & Department of Mechanical Engineering, McGill University, Montréal (Québec), Canada, H3A 0C3*

ibrahim.chamseddine@mail.mcgill.ca
michael.kokkolaras@mcgill.ca

July 2017

Les Cahiers du GERAD
G–2017–57

Abstract: Nanoparticle-based drug delivery is a promising method to increase the therapeutic index of anti-cancer agents with low median toxic dose. The delivery efficiency, corresponding to the fraction of the injected nanoparticles that adhere to the tumor site, depends on nanoparticle size a and aspect ratio AR. Currently, values for these variables are chosen empirically, and may not yield optimal targeted drug delivery. This study applies rigorous optimization to the design of nanoparticles. A preliminary investigation revealed that delivery efficiency increases monotonically with a and AR. However, maximizing a and AR results in non-uniform drug distribution, which impairs tumor regression. Therefore, a multi-objective optimization problem (MO) is formulated to quantify the trade-off between nanoparticles accumulation and distribution. The MO is solved using the derivative-free Mesh Adaptive Direct Search algorithm. Theoretically, the Pareto-optimal set consists of an infinite number of mathematically equivalent solutions to the MO problem. However, interesting design solutions can be identified subjectively, e.g., the ellipsoid with a major axis of 720 nm and an aspect ratio of 7.45, as the solution closest to the utopia point. The MO problem formulation is then extended to optimize nanoparticle biochemical properties, in particular ligand-receptor binding affinity and ligand density. Optimizing physical and chemical properties simultaneously results in optimal designs with reduced nanoparticle sizes, thus enhanced cellular uptake. The presented study provides an insight on nanoparticle structures that have potential for producing desirable drug delivery.

Keywords: Cancer nanotherapy, multi-objective optimization, nanoparticle design

Acknowledgments: The authors would like to thank Prof. Hermann Frieboes from the University of Louisville for his insightful comments. This work has been supported partially by NSERC Discovery Grant 436193-2013; such support does not constitute an endorsement by the sponsor of the opinions expressed in this article.

1 Nomenclature

a	Nanoparticle major axis
AR	Nanoparticle aspect ratio
$c(\mathbf{x})$	Spacial distribution of drug concentration in tumor
D_d	Effective diffusion coefficient of drug in tumor
δ_{eq}	Equilibrium separation distance between nanoparticle and vessel
EC	Drug effective concentration
η	Nanoparticle delivery efficiency
F_s	Drag force coefficient
h_0	Maximum distance between a nanoparticle and vessel
$\mathbf{J}_{\mathrm{NP}}$	Flux of nanoparticles entering the tissue from the blood
K_a^0	Ligand receptor affinity under zero external force
k_B	Boltzmann Constant
ℓ	Vector of vessels' lengths
λ	Characteristic length of the ligand-receptor bond
λ_d	Cellular uptake cofficient of drug by tumor
λ_p	Area fraction of tumor regions that receive drug greater than or equal to the effective dose (this quantity is used as surrogate to the negative of tissue proliferation rate)
M	Molar mass of drug
m_l	Surface density of ligands
m_r	Surface density of receptors
m_{10}	Mass of drug encapsulated in 10 billion nanoparticles
$\dot{N}_{in}$	Nanoparticles inlet flow rate
R	Vector of vessels' radii
σ	Oxygen and nutrients concentration
T	Mean body temperature
T_{inj}	Drug injection time
T_s	Torque coefficient
τ	Wall shear stress in blood vessels
U_{NP}	Speed on nanopartcles in blood
U_∞	Blood speed in parent vessel
$\%wt$	Nanoparticle drug-loading capacity

2 Introduction

Cancer is a group of diseases characterized by the loss of growth control and disruption of tissue organization. Anti-cancer drugs are commonly associated with intolerable side effects due to their high cytotoxicity. This reveals a need to administer them in a controlled targeted manner to eradicate diseased cells while sparing normal ones. Nanotherapy is an emerging treatment which aims at addressing this challenge by encapsulating the drug in nanoparticles, which are delivered via the circulatory system to the tumor site, where the drug is released.

Nanoparticles are subjected to various forces while they circulate the blood vessels, drift toward the vessel walls (marginate), and adhere to the endothelium or internalize to a cancerous tissue where the payload is released.[1] These forces include buoyant, hemodynamic, gravitational, Brownian, and centrifugal loadings, as well as Van der Waals, electrostatic, and steric nanoparticle-to-nanoparticle interaction. Therefore, the nanoparticle mechanical properties considerably affect the overall effectiveness of the treatment [1]. This study focuses on nanoparticle size and shape due to their impact on the flow and adherence of nanoparticles, as explained in Sections 2.1 and 2.2.

[1] This study focuses on endothelium-adhering nanoparticles

2.1 Size effect

Nanoparticle size is an influential factor in the nanoparticle delivery process which successively comprises margination, accumulation, and internalization. Margination is the lateral movement of nanoparticles toward the vessel walls. While marginating, nanoparticles are subjected to hemodynamic, gravitational, Brownian, and centrifugal forces [2]. Experimental [3] and computational [2] studies showed that Brownian forces have dominant effect on the margination of small nanoparticles (diameter less than 500 nm); however, gravitational forces are significant in the margination of bigger nanoparticles. Toy et al. [4] measured the nanoparticle tendency to drift toward the wall in an *in-vitro* microcirculation model. Nanoparticles of diameters {56, 60, 65, 100, 300} nm and aspect ratios {0.45, 1} were considered to show that smaller and oblate-shape nanoparticles are associated with higher margination rates. This complies with the fact that small nanoparticles have stronger Brownian motion, allowing them to escape their streamlines. Bigger nanoparticles (of diameters {200, 500, 2000, 5000} nm), delivered to an *in vitro* parallel flow chamber [5], showed that the margination rate increases as the nanoparticle size increases. Notably, although large nanoparticles enhance margination, they hardly cross the endothelium, thus large size is a limiting factor for the nanoparticle internalization. Decuzzi et al. [6] developed a theoretical model for nanoparticle margination considering buoyant and hemodynamic forces, and van der Waals interactions. The model showed that the lowest margination rate occurs with nanoparticle radii that lies between 50 nm and 200 nm (depending on Hamaker constant). The study suggested using diameters less than 100 nm for drug delivery applications where high margination rates are favorable.

When nanoparticles approach the vessel walls, their ligands (in active targeting) adhere to the receptors of the endothelial cells. The adherence strength depends on the nanoparticle size. The first experimental demonstration for this dependency was done by Patil et al. [7] who used {5, 10, 15, 20} μm diameter microspheres, coated with P-selectin glycoprotein ligands, and measured their accumulation *in vitro*. Decuzzi et al. [8] provided a theoretical model for the probability of a nanoparticle to adhere to a certain vessel as a function of the nanoparticle size and aspect ratio, vessel wall shear stress, and receptor-ligands association constant, among other parameters. The model showed that there exist a nanoparticle size that maximizes the probability of adherence for a given aspect ratio.

Nanoparticles binding firmly to the endothelial layer are transported into the tissue through clathrin-dependent or caveolin-dependent endocytosis [9, 10, 11]. Due to the fact that the absorption of nanoparticles by the tissue is nonphagocytotic, ligand-receptors interaction, and thus nanoparticle structure, plays very important role in nanoparticle internalization. Foged et al. [12] measured the uptake of nano-spheres of diameters {100, 500, 1000, 4500} nm by human denderitic cells in an *in vitro* model. Results showed that small nanoparticles area associated with enhanced uptake rate. Similar conclusion was drawn in [13] and [14] who studied the uptake of particles with diameters ranging from 100 nm to 5 μm by HeLa cells. In parallel, if the drug is released at the endothelium, its transport in the tissue is governed by the diffusion-reaction equation where values about the effective diffusion coefficient and cellular uptake rate are recorded in [15, 16].

The cell-particle interaction model of [8] was integrated in [17] with an *in-silico* models for tumor growth, mechanics, and angiogenesis, which were developed by the successive work of [16, 18, 19]. Spherical nanoparticles of {100, 600, 1000} nm radii were simulated in [17]. Results showed that although large nanoparticles have high delivery efficiency, they accumulate at the tumor inlet, leaving the core free of drug. In contrary, small nanoparticles showed a uniform intra-tumoral distribution but with low adherence strength. Van de Ven et al. [20] expanded this model by adding the effect of drug concentration on the overall tumor proliferation rate in order to examine the number of nanoparticles needed to reach the half maximal effective concentration IC_{50}.

2.2 Shape effect

Nanoparticles are usually produced using bottom-up fabrication methods such as self-assembly and nanoprecipitation. These methods are driven by minimizing energy and molecular self-assembly entropic effects, favoring low aspect ratio structures. For this reason, early nanoparticle studies focused on nanospheres.

Nanoparticle shape, however, plays an important role - besides the size - in nanoparticle margination, adhesion, and uptake, as reviewed in [1].

Eccentric nanoparticles flowing in blood are subjected to non-uniform hydrodynamic loadings across their axes of symmetry, causing them to rotate and deviate from their streamlines. Therefore, spheroids, discs, and rods marginate faster than spheres [3]. Gavze and Shapiro [21] determined the drift velocity of micro-scale spheroids flowing near a solid wall using an analytical model that computes the forces and torques induced by the flow. The study showed that the aspect ratio corresponding to the maximum drift velocity is directly proportional to the flow shear stress. Shah et al. [22] studied nanoparticles of aspect ratios 1 and 5. Results showed that the nanoparticles of higher aspect ratio deviate faster to the vessel wall. The shape effect on margination was also studied in [23] which considered spherical, hemispherical, and discoidal nanoparticles flowing at the same shear rate. Hemispherical nanoparticles was associated with the fastest dispersion, followed by discoidal, and then spherical ones.

High aspect ratio nanoparticles have higher probability to adhere to a vessel wall due to increased contact area - more number of ligands are exposed to more number of receptors. In addition, lodged nanoparticles with such structures are subjected to reduced hemodynamic dissociation loadings. A computational model [8] that measures the strength of adherence as a function of nanoparticle size and shape showed that the probability of a nanoparticle-to-cell adherence increases as the nanoparticle aspect ratio increase. Experiments conducted in [24, 22] showed similar relation between the aspect ratio and binding strength. Finally, accumulated nanoparticles of higher aspect ratio showed facilitated cellular uptake [25]. Such relationship between endocytosis and nanoparticle aspect ratio is modeled in [26].

2.3 The objective of this study

Experimental studies typically focus on producing nanoparticles of small sizes, high entrapment efficiency, high negative zeta potential, and high cumulative drug release. While these studies relate the nanoparticle structure to other nanoparticle properties such as drug-to-shell weight ratio, they do not take into account objectives related to tumor invasion. An alternative approach is to consider nanoparticle structures that enhance margination, accumulation, and endocytosis in order to maximize tumor targeting. Time and cost needed to develop *in vitro* and *in vivo* models are typically high, and further escalated by nanoparticles production cost. Therefore, the development of computational models is beneficial to obtain reproducible results at relatively low cost. These models, however, describe different mechanisms involved in nanoparticle delivery and tumor response in an independent fashion. Thus, using them to design nanoparticles would result in favoring some aspects of nanotherapy, such as enhancing adherence to endothelia or increasing circulation time, rather than improving the overall treatment. In this paper, awe propose an optimization framework for designing nanoparticles with the objective of maximizing tumor targeting, quantified by the delivery efficiency η, defined as the fraction of the injected nanoparticles that adheres to the tumor.

3 Computational model

An analysis model is used to quantify the accumulation of drug carrying nanoparticles (NPs) at the microvasculature of a solid tumor, and drug release into the cancerous cells. The model used here is adapted from models for tumor mechanics and drug delivery, reported in [8, 16, 17, 18, 19, 20]. It consists of flow, accumulation, endocytosis, and tumor growth submodels, that are integrated as shown in Figure 1.

3.1 Tumor structure

The tumor is described in a 2D Cartesian coordinate system as an ellipse with major and minor axes of 1 mm and 0.7 mm respectively (see Figure 2). It is formed of viable tissue able to proliferate if the drug delivered does not exceed as specific threshold. In reality, tumors are formed of viable, necrotic, and hypoxic regions; however, this paper is implementing a simpler, yet more conservative model by considering the entire region viable.

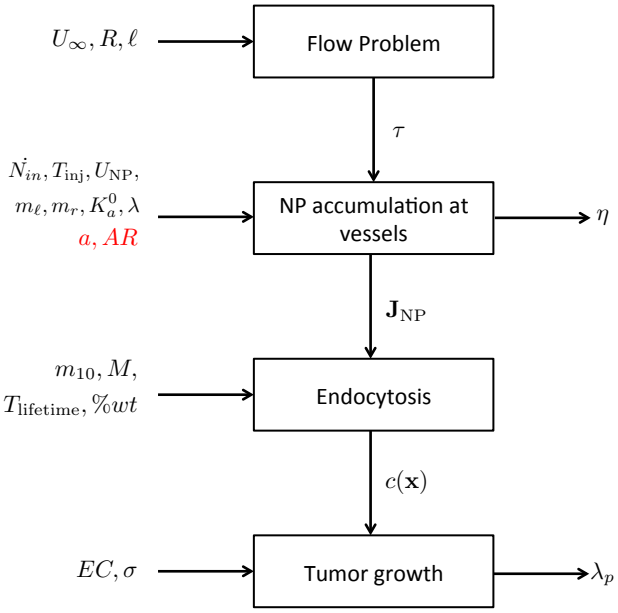

Figure 1: Analysis model

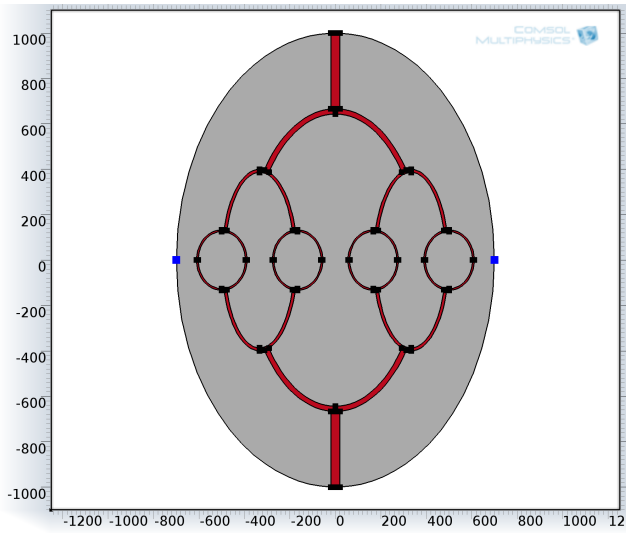

Figure 2: Tumor structure model (dimensions are in μm)

3.2 Tumor vessels

Tumor hypoxic tissue releases tumor angiogenic factors, among other growth factors, to induce angiogenesis. Angiogenesis is a physiological process through which new vessels are generated from pre-existing vessels to supply cancerous cells with oxygen and nutrients. These tumor vessels have chaotic global organization, dilated diameters, poor flow, and heterogeneous vascular density. Angiogenesis is modeled in [18, 27] and integrated with a tumor growth model in [19]. Tumor vessels can be normalized by certain antiangiogenic agents to retrieve the vessel normal structure and function, thus improving the delivery of nanomedicine [28, 29].

This study considers a tumor vasculature that has been exposed to antiangiogenetic therapy. The normalized vessels have fractal properties resembling normal vascular organization [30]. A fractal-based tumor vessel model, developed in [31], estimates a radii ratio between a tumor vessel branch and its daughter branch

as $3^{-0.25}$. Blood capillary radius typically ranges from 2μm to 24μm. In the computational model used here, the vasculature is composed of 4-generation network. For this reason, higher radii ratio is used to engage wider range of capillary sizes (3.85μm to 20μm.) The flow in the capillaries is a creeping flow (very low Reynolds number) driven by an inlet velocity of 0.2mm/s (from below). The flow model considers blood non-newtonian properties, and is implemented in COMSOL Multiphysics Software. The resulting wall shear stress is in the order of $0.1 - 10$ Pa, complying with the physiological data recorded in [8].

3.3 Nanoparticle accumulation

NPs are injected at the tumor inlet. The probability of a NP to adhere to a certain vessel is determined in [8] as

$$P_{adh} = \pi r_0^2 \left(m_r m_l K_a^0\right) \exp\left[-\frac{\lambda}{k_B T}\left[6\left(\frac{a}{AR} + \delta_{eq}\right) F^S + 8\frac{a^2}{r_0} T^S\right] \frac{a}{r_0^2}\frac{\tau}{m_r}\right] \tag{1}$$

Equation (1) accounts for the NP-to-endothelial substrate contact area, NP-endothelium binding affinity, NP Brownian motion, and disassociation forces and torques induced by the blood flow. The rate of NPs attaching at the inlet vessel is $\dot{N} = P_{adh}\dot{N}_{in}$. The rate of NPs leaving the inlet vessel defines $\dot{N}_{in}$ of the daughter vessel. This process is solved successively using MATLAB to determine the number of NPs attached to each vessel per second, thus calculating the delivery efficiency η as the total number of attached NPs to the injected ones. Ultimately, the amount of drug leaking from the tumor should remain below the lowest lethal dose ($\mathrm{LD_{Lo}}$). The values of $\dot{N}$ composes the boundary conditions for the next subproblem - transport of drug in the cancerous tissue.

3.4 Drug transport in the tissue

The model considers drugs that are released to the cancerous tissue from NPs adhering to the endothelium, rather than internalized to the tissu. The drug is transported in the tissue by means of diffusion and cellular uptake mechanisms which is modeled in [16] by the quasi-steady reaction-diffusion equation

$$0 = \nabla \cdot (D_d \nabla c) - \lambda^d c$$

The value of the effective diffusion coefficient D_d is calibrated in [16, 19] to experimental data; however, diffusion anisotropy in tumors is studied in [32]. In addition, detailed studies on cellular uptake mechanisms are available in [9, 15, 33, 34]. The transport of drug in the tumor is solved in COMSOL for Neumann boundary conditions which are obtained in the preceding NP accumulation subproblem.

3.5 Tumor growth

Each mesh in the tumor compartment represents an epithelial cell. Meshes are generated in COMSOL with size ranging from $0.15\mu m$ to $40\mu m$. Cell are subjected to an apoptosis–proliferation effects. Cell apoptosis is modeled in [20] which also accounts for cell proliferation caused by oxygen concentration σ, an effect that is neglected in this study. In normal cells, apoptosis happens naturally with an apoptosis rate A. The value of A is set to zero because malignant cells lose their growth control. In this context, apoptosis is triggered if the concentration of the drug in the cell exceeds a certain threshold (EC). Cellular growth and death effects are quantified by proliferation rate λ_p, which is defined in [17] as

$$\lambda_p = \sigma(1 - (c(\mathbf{x}) - EC)) - A$$

The value of λ_p depict the tumor volume reduction rate. The quantity λ_p refers in this paper to the fraction of area that receives drug more than EC, as a surrogate of tumor proliferation rate.

3.6 Model validation

Frieboes et al. [17] simulated the delivery of nanospheres with diameters of {100, 600, 1000} nm. Each nanoparticle size is simulated using 5 different binding affinities, represented by the parameters α and β, and

the fractions of the accumulated nanoparticles were recorded for the 15 cases. We use our model to simulate these different cases, and the resulting η is compared to the fraction of accumulated nanoparticles in [17].

To compare both models at similar tumor conditions, the average wall shear rate of 19.31 s^{-1} is set as parameter, referring to the tumor stage of day 24 in [17]. The parameters $\alpha \propto m_r m_\ell K_a^0$ and $\beta \propto \lambda\mu/(k_B T m_r)$ are used to calculate m_r and m_ℓ. For example, $\alpha = 10^{10}\mathrm{m}^{-2}$ and $\beta = 10^{-5}\mathrm{m}^{-2}s$ are equivalent to $m_r = 5.14 \times 10^{13}\#/\mathrm{m}^2$ and $m_\ell = 1.95 \times 10^{10}\#/\mathrm{m}^2$ if the proportionality constant is 1. Then, η is computed at $AR = 1$ and $a = \{100, 600, 1000\}$ nm.

To negate the differences in vessel surface areas between the two models, delivery efficiencies resulting from the same α and β are normalized by their mean value. Both models show good agreement, which is quantified by the statistical measure R^2, demonstrated in Figures 3a, 3b, 3c, and 3d. The proportionality constant K used in each simulation is stated in the caption of Figure 3.

The case of $\alpha = 10^8\mathrm{m}^{-2}$ and $\beta = 10^{-4}\mathrm{m}^{-2}s$ is simulated as well; however, R^2 is not quantified because the fraction of nanoparticles accumulated in the tumor is very small, making it difficult to read from [17]. Nevertheless, this reduction in the accumulation rate is also used to validate our model, which similarly shows that the value of η obtained in the case $\alpha = 10^8\mathrm{m}^{-2}$ is significantly lower than the ones obtained in the cases of $\alpha = 10^{10}\mathrm{m}^{-2}$ and $10^{12}\mathrm{m}^{-2}$.

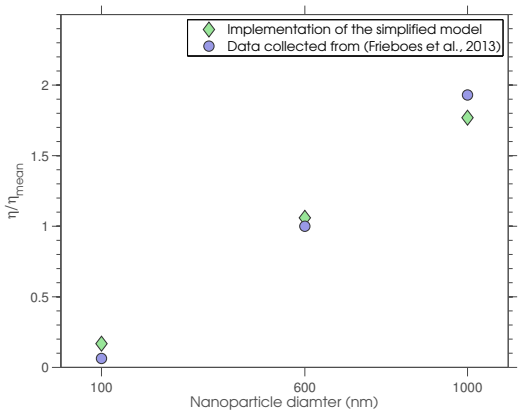

(a) $\alpha = 1 \times 10^{10} m^{-2}, \beta = 1 \times 10^{-5} m^{-2} s, K = 5$, **yields** $\mathbf{R}^2 = 0.9759$

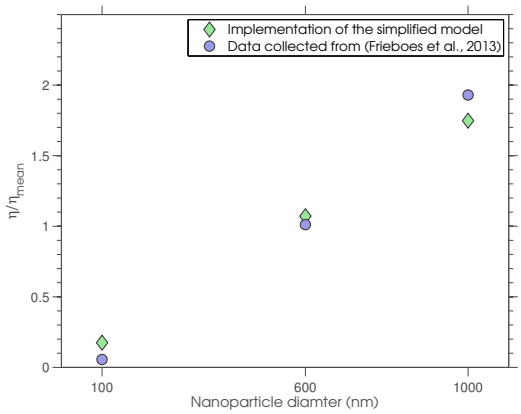

(b) $\alpha = 1 \times 10^{10} m^{-2}, \beta = 1 \times 10^{-4} m^{-2} s, K = 5$, **yields** $\mathbf{R}^2 = 0.9713$

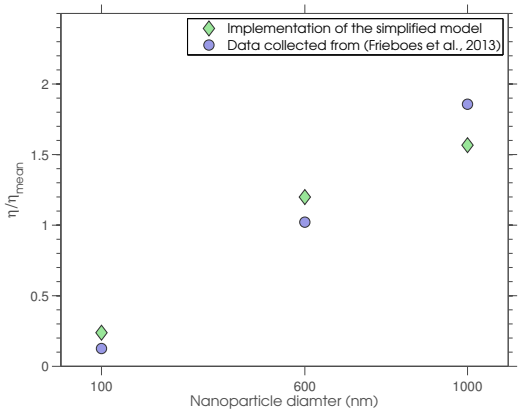

(c) $\alpha = 1 \times 10^{10} m^{-2}, \beta = 1 \times 10^{-3} m^{-2} s, K = 5$, **yields** $\mathbf{R}^2 = 0.9142$

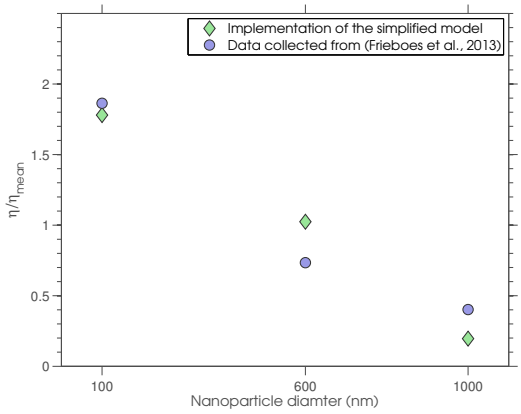

(d) $\alpha = 1 \times 10^{12} m^{-2}, \beta = 1 \times 10^{-4} m^{-2} s, K = 1/25$, **yields** $\mathbf{R}^2 = 0.8845$

Figure 3: Comparison of results obtained with our model with those of that reported in [17]

4 Optimization of nanoparticle size and shape

We first considered the maximizazion of the delivery efficiency η. To that end, a full factorial design-of-experiments was conducted within the design space defined by the constrains imposed on nanoparticle size and aspect ratio. Nanoparticle radius is considered to be greater than 10 nm to avoid renal clearance mechanisms, and below 1000 nm to ensure flow of nanoparticles in narrow tumor vessels. In addition, Nano-spheroids of very large aspect ratios are not considered due manufacturability limitations. Therefore, the aspect ratio is set to range from 1 (sphere) to 10, similar to [8].

Nanoparticles with higher aspect ratio are associated with increased contact area with the endothelial substrate (i.e. higher avidity), and reduced dislodging effect of blood flow. On the other hand, bigger nanoparticles have more contact area with the endothelium, but are subjected to stronger hemodynamic forces and torques. Consequently, there exist a nanoparticle size where the nanoparticle-to-endothelium binding strength is maximum. For the parameters considered in this study, this maximum lies on the boundary of the design space because η increases monotonically with a and AR as shown in Figure 4. This indicates that the delivery efficiency is maximized for a nanoparticle major axis of 1000 nm and aspect ratio of 10.

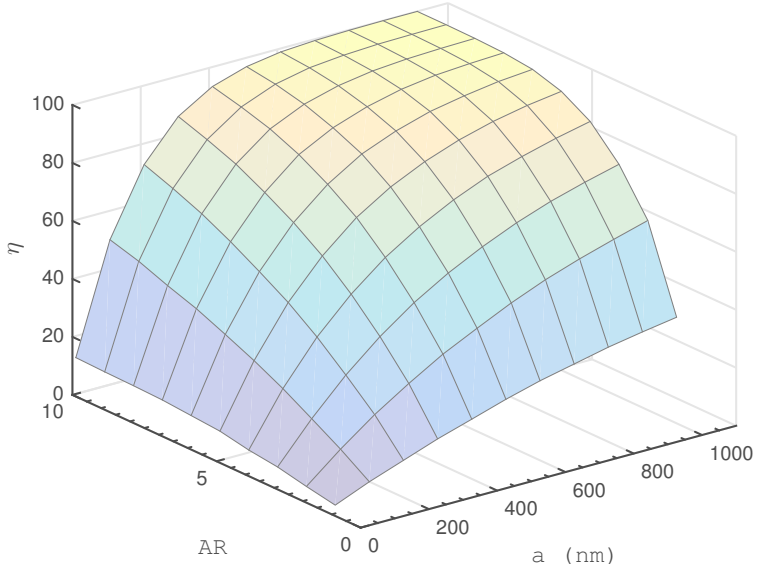

Figure 4: Delivery efficiency as a function of nanoparticle structure

Although maximizing η is ideal for toxicity reasons, it is not favorable in terms of tumor volume reduction rate because nanoparticles tend to accumulate at the tumor entrance and spare the tumor core. This was noticed in [17] by examining the distribution of nanoparticles across the tumor. The nanoparticle distribution is also quantified in this study as shown in Figure 5, which illustrates the number of nanoparticles adhering to each vessel in the vasculature tree after injecting 15,000 NPs. Figure 5b depict the case of delivering the largest and most oblate nanoparticles; i.e, maximum η. It shows that most of the injected NPs adhere at the tumor inlet vessel. When the delivery efficiency is low, the nanoparticles undergo a more uniform distribution but with lower quantities (Figure 5a). This result shows that high delivery efficiency impairs the uniformity of nanoparticle distribution, thus reducing the tumor area that receives enough drug concentration. To mitigate this issue, the multi-objective optimization (MO) problem (2) is formulated considering the area fraction (λ_p) of the regions that receive the effective dose (EC) as an additional objective function to η. For the drug Doxorubicin, EC varies between 10 and 100 μM [20]. In this study, any region that receives more than 20 μM is considered subject to apoptosis.

$$\begin{aligned} \underset{a,AR}{\text{maximize}} \quad & [\eta, \lambda_p] \\ \text{subject to} \quad & 10 \leq a \leq 1000 \text{ (nm)} \\ & 1 \leq AR \leq 10 \end{aligned} \tag{2}$$

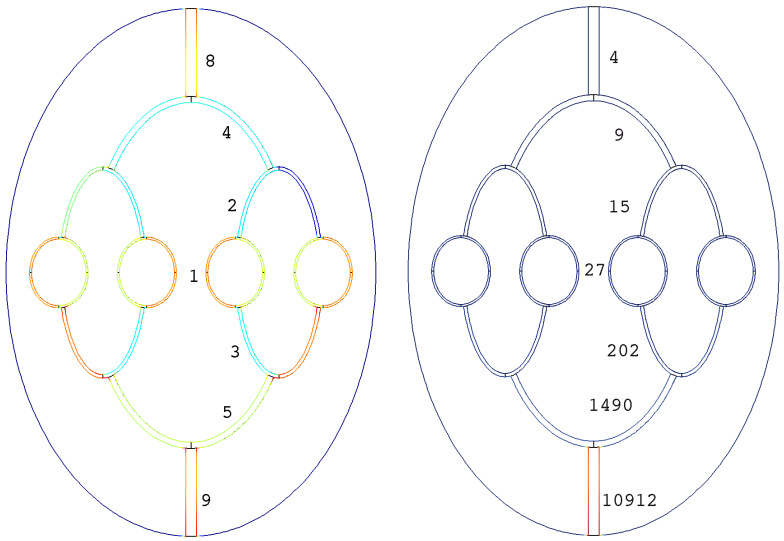

(a) $a = 10$ **nm,** $AR = 1$ **(b)** $a = 1000$ **nm,** $AR = 10$

Figure 5: Number of nanoparticles attached to each level of vessels

Since η and λ_p are computed using simulation models, a gradient-based optimization approach would require an elaborate effort to ensure that the gradients of these two functions with respect to the design variables can be approximated reliably. Moreover, we would need to implement an appropriate methods (such as the ϵ-constraint method) to generate an adequate amount of Pareto points to approximate the Pareto front. Instead, we opted for solving Problem (2) using a derivative-free optimization algorithm. Specifically, we selected the Mesh Adaptive Direct Search algorithm (MADS) [35] because of its rigorous convergence properties and its capability to solve bi-objective problems and generate Pareto-optimal solution sets. The termination criterion is set such that the maximum number of blackbox evaluations for all MADS runs is 20. This is adequate for a two-dimensional problem, and insures a mesh size of less than 1E-2, which is a sufficient approximation because it provides a precision of less than 1 nm for $a^\star$ and less than 0.01 for $AR^\star$.

The solution of the MO (2) is represented in Figure 6 by the Pareto front which consists of the set of optimal solutions that quantify the tradeoff between η and λ. Since it is steep at both ends, the designs corresponding to the two extreme Pareto points $(a = 1000nm, AR = 10)$ and $(a = 553nm, AR = 5)$ should not be considered because a tiny improvement in one objective requires a significant sacrifice from the other. The *utopia* point $[\eta = 100\%, \lambda_p = 55\%]$ is defined by the optimal values that would have been achieved if the two objective functions were not competing, which is not the case in this MO problem. Choosing a Pareto point and the corresponding design is a subjective choice. Here, a design corresponding to a Pareto point close to the utopia point, e.g. $a^\star = 720nm$ and $AR^\star = 7.45$, is selected because it leads to high $\eta^\star = 96.80\%$ and very good distribution $\lambda^\star = 50.31\%$. Using this design, drug distribution increases significantly as compared to maximizing η alone. Both cases are shown in Figure 7, which depicts the tumor regions that receive drug exceeding the EC after 50 seconds from injecting 1,500 NP/s with an injection duration of 10 seconds.

4.1 Multiple optimizers

There is a possibility that other combinations of a and AR lead to the same Pareto point $(\eta = 96.8\%, \lambda_p = 50.31\%)$. To check for the presence of multiple optima, the optimization problem

$$\begin{aligned} \underset{a,AR}{\text{minimize}} \quad & f = (\eta - 96.8)^2 + (\lambda_p - 50.31)^2 \\ \text{subject to} \quad & 10 \leq a \leq 1000 \text{ (nm)} \\ & 1 \leq AR \leq 10 \end{aligned} \tag{3}$$

is solved using NOMAD. The optimal solutions obtained using different initial guesses are listed in Table 1, which shows that the set of minimizers is not a singleton.

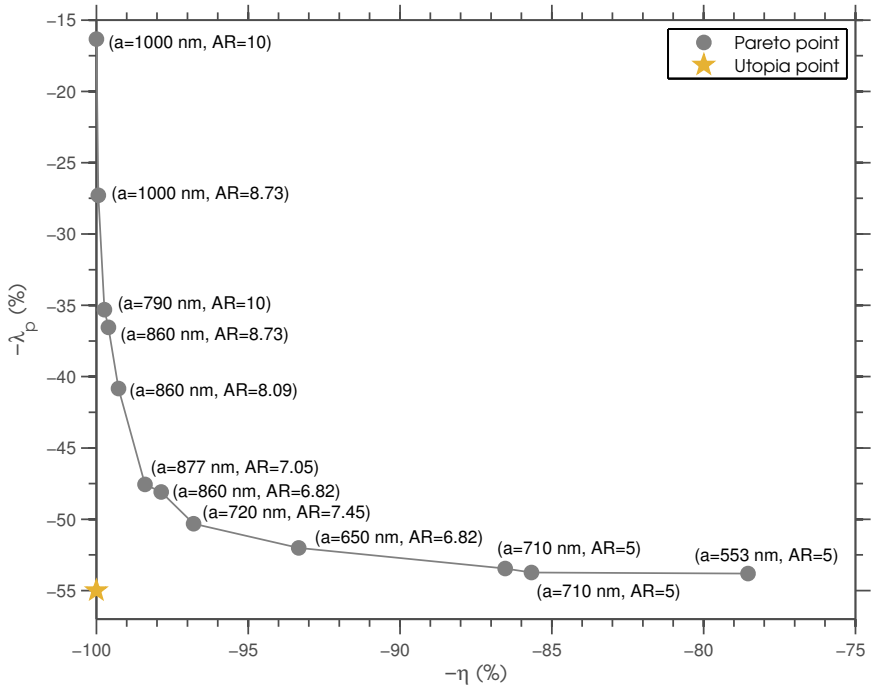

Figure 6: Pareto front referring to the tradeoff between η and λ_p

Table 1: Solution of Problem (3)

Initial Guess		Optimal Solution			
a_0 (nm)	AR_0	$a^\star$ (nm)	$AR^\star$	$\eta^\star(\%)$	$\lambda_p^\star(\%)$
500	5	982.5	5.64	96.8	50.2268
500	10	605	9.054	97.0667	50.13

Figure 8 depicts the isocontours of η over the design space using a full factorial DoE with 100 points. The shape of the isocontours indicates that, at constant η, the nanoparticle design varies from being small and oblate to large and more spherical. For $\eta = 96.8\%$, nanoparticles range from ($a = 1000$nm, $AR = 5.58$) to ($a = 560$nm, $AR = 10$) over a path that is defined by the isocontour. Large isotropic nanoparticles are easier to manufacture, but harder to be uptaken by the tissue. In other words, the isocontours demonstrate a tradeoff between facilitating endocytosis and manufacturability. From this spectrum, the result obtained by the Pareto front of the MO (2), i.e ($a = 720$nm, $AR = 7.45$), maintains a good balance between η and λ_p. Note that the model does not consider the effect of nanoparticle structure on endocytosis, but rather considers that the drug is released at the endothelium. More details on the size and shape effects on endocytosis are found in [1, 26, 25].

4.2 Sensitivity of the optimal solution

A parametric study is conducted to investigate the effect of the tumor vessels conditions, characterized by the wall shear stress, on the optimal nanoparticle design. Different values of τ represent different tumor stages or microenviroments. Note that this study is not an attempt to account for tumor heterogeneity, but an investigation for the sensitivity of the optimal design as the flow parameters change due to tumor progression/regression. Figure 9 plots the Pareto points using the average wall shear stress $\bar{\tau}$ studied so far, and its perturbation by $\pm 10\%$ and $\pm 20\%$. It shows that, for all the cases considered, a nanoparticle size of 720 nm and aspect ratio of 7.45 result in a point close to the utopia point. The proximity of these design points implies that the obtained optimal solution is insensitive to moderate changes in the tumor structure.

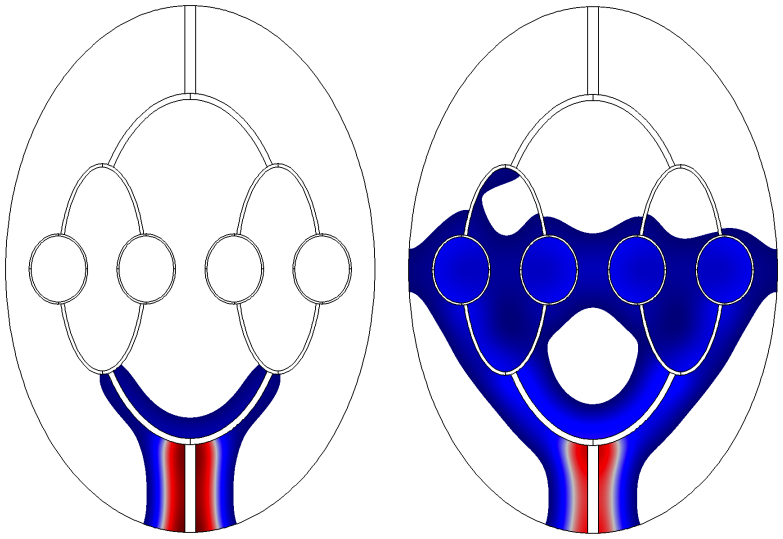

(a) Single objective optimization: $a^\star = 1000nm, AR^\star = 10, \eta^\star = 99.98\%, \lambda_p = 16.2\%$

(b) Multi-objective optimization: $a^\star = 720nm, AR^\star = 7.45, \eta^\star = 96.80\%, \lambda_p^\star = 50.31\%$

Figure 7: Areas that received drug exceeding $EC = 20\mu M$ after 50 seconds from transporting in the tissue

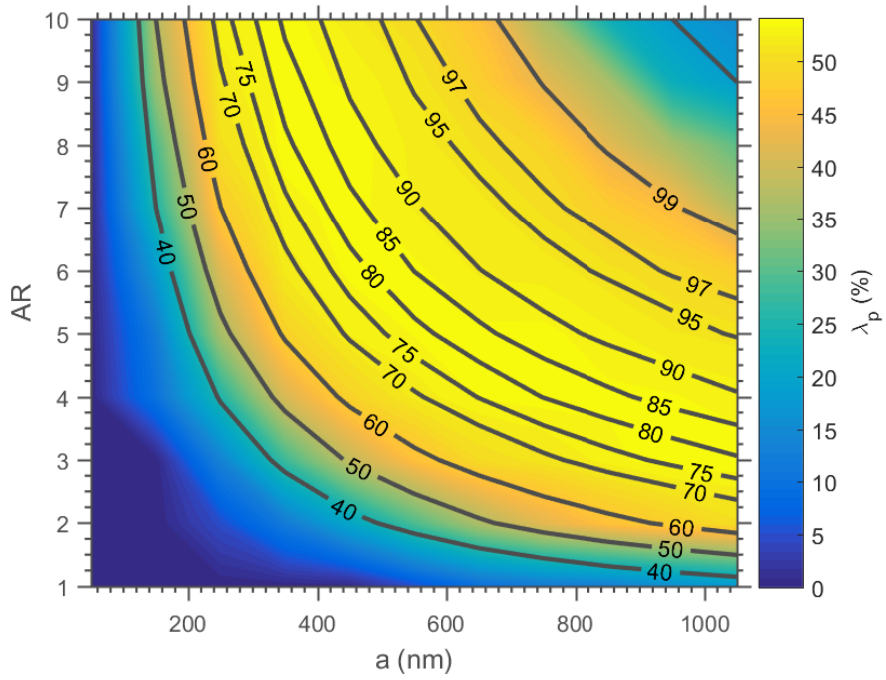

Figure 8: The isocontours of η are shown in black curves labeled by their values. The design space is shaded by the values of λ_p which are defined by the color-bar on the right of the figure

5 Extending the optimization framework to account for chemical properties

5.1 Active targeting

In active targeting, nanoparticles are decorated with ligands having high binding affinities to receptors that are over expressed in malignant tissues. Receptors ($\mathfrak{R}$) are proteins that receive chemical signals from outside the

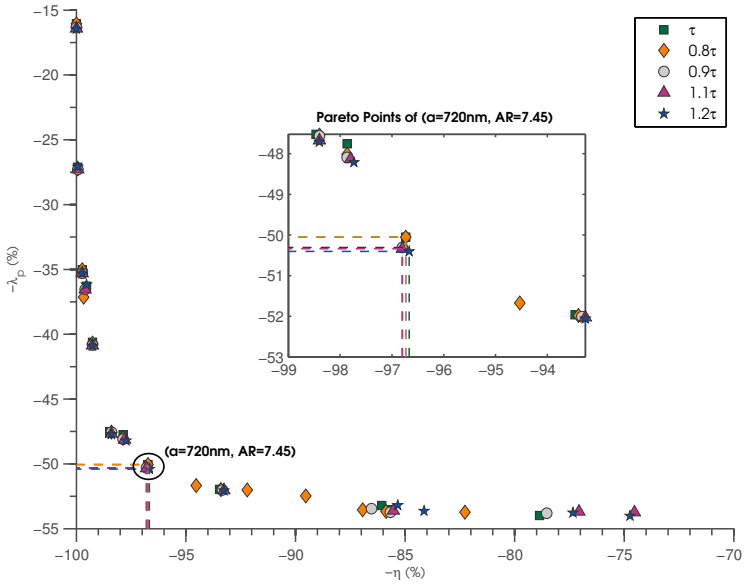

Figure 9: Pareto points corresponding to different average wall shear stresses in the tumor vessels

cell, causing cellular responses. Ligands ($\mathfrak{L}$) are molecules that bind to a central atom to form a coordination complex. The propensity of a ligand to a receptor is given by the chemical reaction $\mathfrak{R} + \mathfrak{L} \rightarrow \mathfrak{RL}$. The kinetics of the chemical reaction is measured by the Binding Constant which defines the affinity and avidity of a ligand-receptor pair. Affinity is the binding strength of a single ligand to a single receptor. Avidity, is the added strengths of all affinities. In this context, the avidity refers to overall strength of binding a nanoparticle to the endothelium.

Integrins are receptors that bind cells together and with the cellular matrix. The integrin $\alpha_v\beta_3$ is distributed in endothelial cells, melanoma, and glioblastoma. The corresponding ligands include Vitronectin [36], glycoprotiens such as fibronectin and fibrinogen, and proteins which include osteopontin and Cyr61. In addition, ligands can be designed to have enhanced binding kinetics with $\alpha_v\beta_3$-integrin. A novel example for such synthesized ligands is the ProAgio protein which is developed by Turaga et al. [37].

In addition to the integrin $\alpha_v\beta_3$, E-selectin (CD62E) is used to mark tumor vessels. E-selectin is a cell adhesion molecule, encoded by *SELE* gene, that is expressed in the endothelial cells [38]. In cancer cells, many molecules are identified as E-selectin ligands such as the glycoprotiens CD44, ESL-1, and PSGL-1 [39, 40].

Recent studies show that active targeting enhances the performance of nanoparticle-based drug delivery. For instance, drug-loaded poly lactice-co-glycolic acid (PLGA) nanoparticles, equipped with monoclonal antibody active reagent (mAb) ligands, caused tumor volume reduction in mice ovarian cancer, as compared to only slowing down the growth of tumor in the absence of ligands. Suh et al [41] used the biocompatible polymer ligands: hyaluronic acid CD44 targeting moiety, and chitosan physical cross-linker. Results showed that active targeting was associated with 8-fold increase in drug specificity when compared with conventional intravenous injection.

5.2 Augmenting the design variables of the optimization problem

One of the many advantages of using optimization in the design of NPs is to obtain the optimal values of multiple design variables at once, as compared to 1 variable per empirical study. Previous sections were focusing on designing the NPs physical properties assuming specific ligand-receptor pair and densities. While there is no control over the receptors properties in the endothelium ($\alpha_v\beta_3$–integrins are expressed and $m_r \sim 10^{14}\#/\text{m}^2$ [8]), the nanoparticles biochemical properties can be optimized. These properties include the ligands density m_ℓ and the zero-load affinity constant K_a^0. The no-load avidity per receptor ($A_c m_\ell K_a^0$) is positive and considered to be less than $0.26\mu m^2$ [42], where A_c is the contact area between a nanoparticle

and the endothelium ($A_c \approx \pi a^2[1-(1-(h_0-\delta_{eq})AR/a)^2]$). In particular, typical values for per E-selectin cellular avidity range from 0.014 to 0.0511 μm^2 [42]. The no-load avidity of HL-60 cells adhesion to P-selectin is $0.03\mu m^2$ [42], similar to that of Colo-205 adhesion with E-selectin. Another term that is constrained in the optimization problem is the product $m_r m_\ell K_a^0$ which is set to be between 10^8 and 10^{12} as in [17]. The multi-objective optimization problem formulation with respect to nanoparticle physical and chemical properties becomes

$$\begin{array}{lll} \underset{a,AR,m_\ell,K_a^0}{\text{maximize}} & [\eta, \lambda_p] & \\ \text{subject to} & 10 \le a \le 1000 & (nm) \\ & 1 \le AR \le 10 & \\ & 0 \le A_c m_\ell K_a^0 \le 0.26 & (\mu m^2) \\ & 10^8 \le m_r m_\ell K_a^0 \le 10^{12} & (m^{-2}) \end{array} \tag{4}$$

The Pareto front resulted from solving Problem (4) is presented in Figure 10, which also includes the Pareto front of Figure 6 for comparison. The optimizers A, B and C have similar chemical properties. Their $a^\star \sim 300-450$nm is significantly less than that of Problem (2), which is in the range of $700-800$ nm. This indicates that if ligands with $m_\ell \ge 10\ \#/\mu m^2$ and $K_a^0 \ge 1\times 10^{-15}\ m^2$ are used, the optimal solution can have a reduced nanoparticle size, thus better endocytosis.

On the other hand, the divergence in the values of $m_\ell^\star$ and $K_a^{0\star}$ from points A, B, and C to point D means that a low receptor-ligand binding affinity is compensated by increased ligand surface density. Optimizing physical and chemical variables in an all-in-one problem provides insight on the nanoparticle structures suitable for a specific $K_a^{0\star}$ and $m_\ell^\star$, properties that are not necessarily constant but harder to control than a and AR.

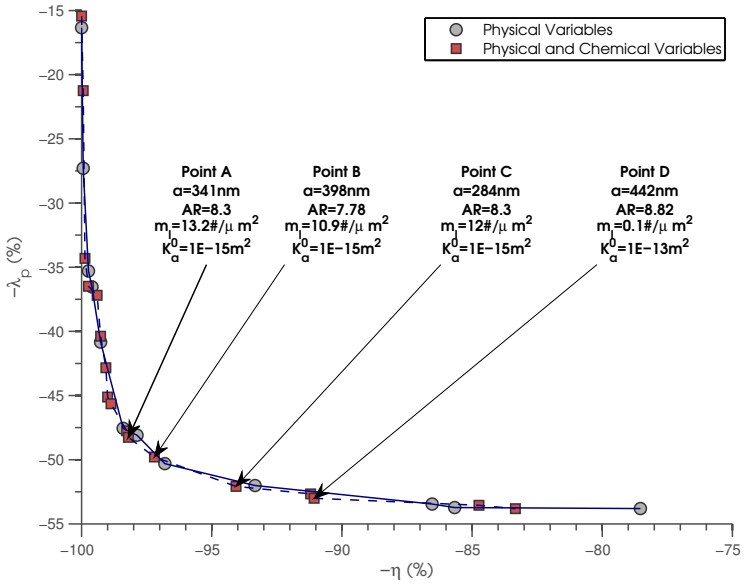

Figure 10: Pareto fronts referring to the cases of optimizing only physical properties, and physical and chemical properties

6 Conclusion

We proposed an optimization-based methodology for designing nanoparticles (NPs) that enhance targeted anti-cancer drug delivery. Preliminary design-of-experiments demonstrated that delivery efficiency increases monotonically with nanoparticle size and aspect ratio. However, maximizing a and AR yields nonuniform nanoparticle distribution across tumor tissue, impairing the overall effectiveness of drug delivery. A bi-objective design optimization problem was formulated to consider drug distribution, and solved using the

derivative-free Mesh Adaptive Direct Search algorithm. A parametric study with respect to the average wall shear stress verified that the optimal solution is insensitive to moderate changes in the tumor microenviroment. The bi-objective optimization problem was then extended to consider design variables associated woth chemical properties.

A modeling assumption was that NP loading capacity is constant; however, in reality, it decreases with particle size as was shown empirically in [43, 44, 45, 46]. Also, many tumor structural parameters were set to fixed values. Tumor structure is heterogeneous, and varies from a tumor to another, or through the progression of the same neoplasm. Hence, a methodology to account for such variabilities during the process of NP design is needed. Future work will include uncertainty quantification of tumor structure to provide a robust nanoparticle design that is suitable for wide range of solid tumors.

To the best of the authors' knowledge, the work presented here is the first application of numerical optimization to the design of drug-loaded nanoparticles. In addition to obtaining optimal NP designs, the field of nanoparticle drug delivery can benefit from optimization in additional ways. In recent studies, nanoparticle properties, such as polymer concentration and drug-to-polymer ratio, were selected empirically to optimize a set of competing fators such as NP size, entrapment efficiency, yield and negative zeta potential [43, 44, 45, 46]. In order to avoid unnecessary particle size reduction, the outcomes of our research can help in setting the lower bound for the nanoparticle sizes that are relevant for anti-cancer drug delivery, thus accommodating larger entrapment efficiency, yield, and negative zeta potential. Moreover, experiments conducted to study nanoparticles flow, accumulation, internalization, and lodging in neovasculature, as well as studies to measure nanoparticle delivery efficiency, pharmacokinetics, and pharmacodynamics are either assuming that NP structure is a parameter set to a fixed value, or are varying NP structure over a course of finite number of relatively expensive and technically complicated trials. The outcome of these experiments, especially the ones related to delivery efficiency, strongly depends on the size and shape of the injected particles, as articulated earlier in this article. This study provides a means for suggesting nanoparticle structure candidates to be considered by experimentalists in more elaborate investigations. Finally, the building blocks of targeted drug delivery systems include entrapment efficiency, drug delivery efficiency, injection pattern, tumor proliferation rate, nanoparticle capacity, and drug release profile. These components are being studied independently because each of them defines a set of complicated research questions. However, optimization algorithms are capable to integrate many of these design problems in a bigger and more realistic drug delivery system-of-systems.

References

[1] A. Sen Gupta, "Role of particle size, shape, and stiffness in design of intravascular drug delivery systems: insights from computations, experiments, and nature," Wiley Interdisciplinary Reviews: Nanomedicine and Nanobiotechnology, 8(2), 255–70, 2016.

[2] S.-Y. Lee, M. Ferrari, and P. Decuzzi, "Shaping nano-/micro-particles for enhanced vascular interaction in laminar flows," Nanotechnology, 20(49), p. 495101, 2009.

[3] F. Gentile, A. Curcio, C. Indolfi, M. Ferrari, and P. Decuzzi, "The margination propensity of spherical particles for vascular targeting in the microcirculation," Journal of Nanobiotechnology, 6(1), p. 9, 2008.

[4] R. Toy, E. Hayden, C. Shoup, H. Baskaran, and E. Karathanasis, "The effects of particle size, density and shape on margination of nanoparticles in microcirculation," Nanotechnology, 22(11), p. 115101, 2011.

[5] P. Charoenphol, S. Mocherla, D. Bouis, K. Namdee, D. J. Pinsky, and O. Eniola-Adefeso, "Targeting therapeutics to the vascular wall in atherosclerosis-carrier size matters," Atherosclerosis, 217(2), 364–370, 2011.

[6] P. Decuzzi, S. Lee, B. Bhushan, and M. Ferrari, "A theoretical model for the margination of particles within blood vessels," Annals of Biomedical Engineering, 33(2), 179–190, 2005.

[7] V. R. S. Patil, C. J. Campbell, Y. H. Yun, S. M. Slack, and D. J. Goetz, "Particle diameter influences adhesion under flow," Biophysical Journal, 80, 1733–1743, 2001.

[8] P. Decuzzi and M. Ferrari, "The adhesive strength of non-spherical particles mediated by specific interactions," Biomaterials, 27(30) 5307–14, 2006.

[9] S. D. Conner and S. L. Schmid, "Regulated portals of entry into the cell," Nature Review Article, 422, 37–44, 2003.

[10] J. P. Best, Y. Yan, and F. Caruso, "The role of particle geometry and mechanics in the biological domain," Advanced Healthcare Materials, 1(1) 35–47, 2012.

[11] J. Wang, J. D. Byrne, M. E. Napier, and J. M. DeSimone, "More effective nanomedicines through particle design," Small, 7(14) 1919–1931, 2011.

[12] C. Foged, B. Brodin, S. Frokjaer, and A. Sundblad, "Particle size and surface charge affect particle uptake by human dendritic cells in an in vitro model," International Journal of Pharmaceutics, 298(2) 315–322, 2005.

[13] S. Muro, C. Garnacho, J. A. Champion, J. Leferovich, C. Gajewski, E. H. Schuchman, S. Mitragotri, and V. R. Muzykantov, "Control of endothelial targeting and intracellular delivery of therapeutic enzymes by modulating the size and shape of icam-1-targeted carriers," Molecular Therapy, 16(8) 1450–1458, 2008.

[14] S. E. A. Gratton, P. A. Ropp, P. D. Pohlhaus, J. C. Luft, V. J. Madden, M. E. Napier, and J. M. DeSimone, "The effect of particle design on cellular internalization pathways," Proceedings of the National Academy of Sciences, 105(33) 11 613–11 618, 2008.

[15] B. D. Weinberg, R. B. Patel, A. A. Exner, G. M. Saidel, and J. Gao, "Modeling doxorubicin transport to improve intratumoral drug delivery to rf ablated tumors," Journal of Controlled Release, 124(1-2), 11–19, 2007.

[16] M. Wu, H. B. Frieboes, S. R. McDougall, M. A. Chaplain, V. Cristini, and J. Lowengrub, "The effect of interstitial pressure on tumor growth: coupling with the blood and lymphatic vascular systems," Journal of Theoretical Biology, 320, 131–51, 2013. [Online]. Available: http://www.ncbi.nlm.nih.gov/pubmed/23220211

[17] H. B. Frieboes, M. Wu, J. Lowengrub, P. Decuzzi, and V. Cristini, "A computational model for predicting nanoparticle accumulation in tumor vasculature," PLoS ONE, 8(2) p. e56876, 2013.

[18] S. R. McDougall, A. R. A. Anderson, and M. A. J. Chaplain, "Mathematical modelling of dynamic adaptive tumour-induced angiogenesis: Clinical implications and therapeutic targeting strategies," Journal of Theoretical Biology, 241(3) 564–589, 2006.

[19] P. Macklin, S. McDougall, A. R. Anderson, M. A. Chaplain, V. Cristini, and J. Lowengrub, "Multiscale modelling and nonlinear simulation of vascular tumour growth," J Math Biol, 58(4–5) 765–98, 2009. [Online]. Available: http://www.ncbi.nlm.nih.gov/pubmed/18781303

[20] A. L. van de Ven, M. Wu, J. Lowengrub, S. R. McDougall, M. A. Chaplain, V. Cristini, M. Ferrari, and H. B. Frieboes, "Integrated intravital microscopy and mathematical modeling to optimize nanotherapeutics delivery to tumors," AIP Adv, 2(1) p. 11208, 2012. [Online]. Available: http://www.ncbi.nlm.nih.gov/pubmed/22489278

[21] E. Gavze and M. Shapiro, "Motion of inertial spheroidal particles in a shear flow near a solid wall with special application to aerosol transport in microgravity," Journal of Fluid Mechanics, 371, 59–79, 1998.

[22] S. Shah, Y. Liu, W. Hu, and J. Gao, "Modeling particle shape-dependent dynamics in nanomedicine," Journal of Nanoscience and Nanotechnology, 11(2) 919–928, 2011.

[23] F. Gentile, C. Chiappini, D. Fine, R. C. Bhavane, M. S. Peluccio, M. M.-C. Cheng, X. Liu, M. Ferrari, and P. Decuzzi, "The effect of shape on the margination dynamics of non-neutrally buoyant particles in two-dimensional shear flows," Journal of Biomechanics, 41(10) 2312–2318, 2008.

[24] L. Tao, W. Hu, Y. Liu, G. Huang, B. D. Sumer, and J. Gao, "Shape-specific polymeric nanomedicine: emerging opportunities and challenges," Experimental Biology and Medicine, 236(1) 20–29, 2011.

[25] S. Salatin, S. Maleki Dizaj, and A. Yari Khosroushahi, "Effect of the surface modification, size, and shape on cellular uptake of nanoparticles," Cell Biol Int, 39(8) 881–90, 2015.

[26] P. Decuzzi and M. Ferrari, "The role of specific and non-specific interactions in receptor-mediated endocytosis of nanoparticles," Biomaterials, 28(18) 2915–2922, 2007.

[27] M. Chaplain, S. McDougall, and A. Anderson, "Mathematical modeling of tumor-induced angiogenesis," Annual Review of Biomedical Engineering, 8, 233–258, 2006.

[28] V. P. Chauhan, T. Stylianopoulos, J. D. Martin, Z. Popovi, O. Chen, W. S. Kamoun, M. G. Bawendi, D. Fukumura, and R. K. Jain, "Normalization of tumour blood vessels improves the delivery of nanomedicines in a size-dependent manner," Nature Nanotechnology, 7(6) 383–388, 2012.

[29] R. K. Jain, "Normalization of tumor vasculature: An emerging concept in antiangiogenic therapy," Science Review, 307, 58–63, 2005.

[30] Y. Gazit, J. W. Baish, N. Safabakhsh, M. Leunig, L. T. Baxter, and R. K. Jain, "Fractal characteristics of tumor vascular architecture during tumor growth and regression," Microcirculation, 4, 395–402, 1997.

[31] K. Leu, G. B. West, A. B. Herman, and V. M. Savage, "Using fractal geometry and universal growth curves as diagnostics for comparing tumor vasculature and metabolic rate with healthy tissue and for predicting responses to drug therapies," Discrete and Continuous Dynamical Systems - Series B, 18(4) 1077–1108, 2013.

[32] T. Stylianopoulos, B. Diop-Frimpong, L. L. Munn, and R. K. Jain, "Diffusion anisotropy in collagen gels and tumors: The effect of fiber network orientation," Biophysical Journal, 99(10) 3119–3128, 2010.

[33] N. D. Evans, R. J. Errington, M. Shelley, G. P. Feeney, M. J. Chapman, K. R. Godfrey, P. J. Smith, and M. J. Chappell, "A mathematical model for the in vitro kinetics of the anti-cancer agent topotecan," Mathematical Biosciences, vol. 189(2) 185–217, 2004.

[34] I. Sorrell, R. J. Shipley, V. Hearnden, H. E. Colley, M. H. Thornhill, C. Murdoch, and S. D. Webb, "Combined mathematical modelling and experimentation to predict polymersome uptake by oral cancer cells," Nanomedicine: Nanotechnology, Biology and Medicine, 10(2) 339–348, 2014.

[35] S. Le Digabel, "Algorithm 909: Nomad: Nonlinear optimization with the mads algorithm," ACM Trans Math Softw, 37(4) 1–15, 2011.

[36] P. Hermann, M. Armant, E. Brown, M. Rubio, H. Ishihara, D. Ulrich, R. Caspary, F. Lindberg, R. Armitage, C. Maliszewski, G. Delespesse, and M. Sarfati, "The vitronectin receptor and its associated cd47 molecule mediates proinflammatory cytokine synthesis in human monocytes by interaction with soluble cd23," The Journal of Cell Biology,, 144(4) 767–775, 1999.

[37] R. C. Turaga, L. Yin, J. J. Yang, H. Lee, I. Ivanov, C. Yan, H. Yang, H. E. Grossniklaus, S. Wang, C. Ma, L. Sun, and Z. R. Liu, "Rational design of a protein that binds integrin alphavbeta3 outside the ligand binding site," Nat Commun, 7, p. 11675, 2016.

[38] T. Collins, A. Williams, G. I. Johnston, J. Kim, R. Eddy, T. ShowsII, M. Gimbrone, and M. Bevilacqua, "Structure and chromosomal location of the gene for endothelial-leukocyte adhesion molecule 1," The Journal of Biological Chemistry, 266(4) 2466–2473, 1991.

[39] R. Kannagi, M. Izawa, T. Koike, K. Miyazaki, and N. Kimura, "Carbohydrate-mediated cell adhesion in cancer metastasis and angiogenesis," Cancer Science, 95(5) 377–384, 2004.

[40] V. S. Shirure, T. Liu, L. F. Delgadillo, C. M. Cuckler, D. F. Tees, F. Benencia, D. J. Goetz, and M. M. Burdick, "Cd44 variant isoforms expressed by breast cancer cells are functional e-selectin ligands under flow conditions," Am J Physiol Cell Physiol, 308(1) C68–78, 2015.

[41] M. S. Suh, J. Shen, L. T. Kuhn, and D. J. Burgess, "Layer-by-layer nanoparticle platform for cancer active targeting," Int J Pharm, 517(1–2) 58–66, 2016.

[42] J. W. Piper, R. A. Swerlick, and C. Zhu, "Determining force dependence of two dimensional receptor-ligand binding affinity by centrifugation," Biophysical Journal, 74, p. 492513, 1998.

[43] A. A. Elsaid Ali, M. Taher, and F. Mohamed, "Microencapsulation of alpha-mangostin into plga microspheres and optimization using response surface methodology intended for pulmonary delivery," Journal of Microencapsulation, 30(8) 728–740, 2013.

[44] S. Asghar, J. M. M. Salmani, W. Hassan, Y. Xie, F. Meng, Z. Su, M. Sun, Y. Xiao, and Q. Ping, "A facile approach for crosslinker free nano self assembly of protein for anti-tumor drug delivery: Factors optimization, characterization and in vitro evaluation," European Journal of Pharmaceutical Sciences, 63, 53–62, 2014.

[45] P. Boonyasirisri, U. Nimmannit, P. Rojsitthisak, S. Bhunchu, and P. Rojsitthisak, "Optimization of curcuminoid-loaded plga nanoparticles using box-behnken statistical design," Journal of Nano Research, 33, 60–71, 2015.

[46] M. A. Akl, A. Kartal-Hodzic, T. Oksanen, H. R. Ismael, M. M. Afouna, M. Yliperttula, A. M. Samy, and T. Viitala, "Factorial design formulation optimization and invitro characterization of curcumin-loaded plga nanoparticles for colon delivery," Journal of Drug Delivery Science and Technology, 32, 10–20, 2016.